


Minimum model for the main feature of shock Hugoniot near its maximum compression ratioJingxiang Shen^{*} and Wei Kang[†]*HEDPS, Center for Applied Physics and Technology, and College of Engineering, Peking University, Beijing 100871, China* (Received 27 July 2022; revised 2 November 2022; accepted 13 December 2022; published 3 January 2023)

When being compressed by a single shock, most materials show a maximum compression ratio beyond the ideal-gas limit of four. In most cases, this phenomenon has long been conjectured to originate from the ionization of core electrons, but a clear physical picture is still lacking. Here we present a simple illustration from the energy-band picture of dense plasmas, where the total energy includes only the contributions from ionization of the bound electrons in addition to those from ideal-gas-like free particles. This additional energy term (ionization energy) directly leads to an additional term in the compression ratio η , which gives a peak on the Hugoniot adiabat. Furthermore, peaks given by different bound states are shown to add linearly ($\eta \approx 4 + \sum_i \Delta\eta_i$), yielding multi-peaked Hugoniots. Quantitative predictions regarding those Hugoniot peaks can be provided systematically by using this minimum model, showing a good agreement with first-principles calculations and experimental data.

DOI: [10.1103/PhysRevB.107.035102](https://doi.org/10.1103/PhysRevB.107.035102)**I. INTRODUCTION**

Shock compression of materials is involved in various situations like inertial confinement fusion [1,2], astrophysical processes [3], and the study of warm and hot dense matter [4]. The initial and final states before and after the pass of a single shock are related by the Rankine-Hugoniot relation [5], $E - E_0 = (1/2)(p + p_0)(V_0 - V)$, which is the direct consequence of mass, momentum, and energy conservations. Here, E , p , and V stand for the internal energy, pressure, and volume of the postshock state, and the subscript “0” denotes the preshock state. This relation is well known to imply an upper bound for the compression ratio $V_0/V \equiv \rho/\rho_0 \equiv \eta$. For example, the ideal-gas equation of state (EOS) yields a maximum compression ratio $\eta = 4$ with this relation.

Since a strong enough shock turns everything into an ideal-gas-like state [6], the Hugoniot adiabat always approaches $\eta = 4$ under the strong shock limit (radiation energy not considered). However, most real-world materials have “peaks” on the Hugoniot, as suggested by experiments and computational EOS studies—the compression ratio would show one or more local maxima where its value significantly exceeds four before finally approaching the ideal-gas limit [7–9]. This is an important feature of EOS in the warm or hot-dense region, and has drawn much attention since decades ago in the study of shock-compressed deuterium [7,10–12].

Since the Hugoniot is determined solely by the EOS, these peaks should emerge naturally if the underlying EOS is modeled properly, either by first-principles calculations [9,13,14] or analytical models [15–19]. However, in most cases those numerical or analytical EOS’s are rather complicated, involving many subtle effects so as to pursue higher accuracy and

a wider applicable range. This makes it difficult to single out the most important underlying physics for these peaks.

At the other extreme, a qualitative but quite reasonable explanation exists (see, for example, Ref. [13]). For ideal gas, all the $p\Delta V$ work turns into kinetic energy E_k of particles and contributes to pressure as $2E_k/(3V)$. However, for real materials, some internal degrees of freedom may get excited as temperature raises, such as ionization of core electrons or molecular dissociation. These additional energy-absorption mechanisms reduce the proportion of total absorbed energy being converted to E_k , making the material have lower pressure, i.e., being more compressible than an ideal gas. This explanation captures the key physics in general, but there is still a gap in between—how precisely an energy-absorbing process (like ionization) gives rise to a peak on the Hugoniot? Do these peaks have a universal profile? And, how are their positions and sizes related to the number and energy levels of the bound electrons?

In this paper, we would like to present a simple but universal illustration on the origin of these peaks by using the energy-band picture of dense plasmas. We show that ionization of every bound level would directly give rise to a peak on the Hugoniot. In addition, contributions from different bound levels $\Delta\eta_i$ are shown to add linearly to give the overall compression ratio exceeding four ($\eta \approx 4 + \sum_i \Delta\eta_i$, where the subscript i denotes the numeration of different bound levels). Using this model, some global trends in which the preshock density, ionization energy, numbers of bound and free electrons, etc. may affect the peak heights (hence the maximum compression ratio) are presented in a general way.

II. A SINGLE BOUNDED STATE

Electron orbitals in hot dense plasmas can be characterized as being bound or free in general [20]. Since thermal ionization of inner-shell electrons absorbs much more energy

^{*}shenjingxiang93@pku.edu.cn[†]weikang@pku.edu.cn

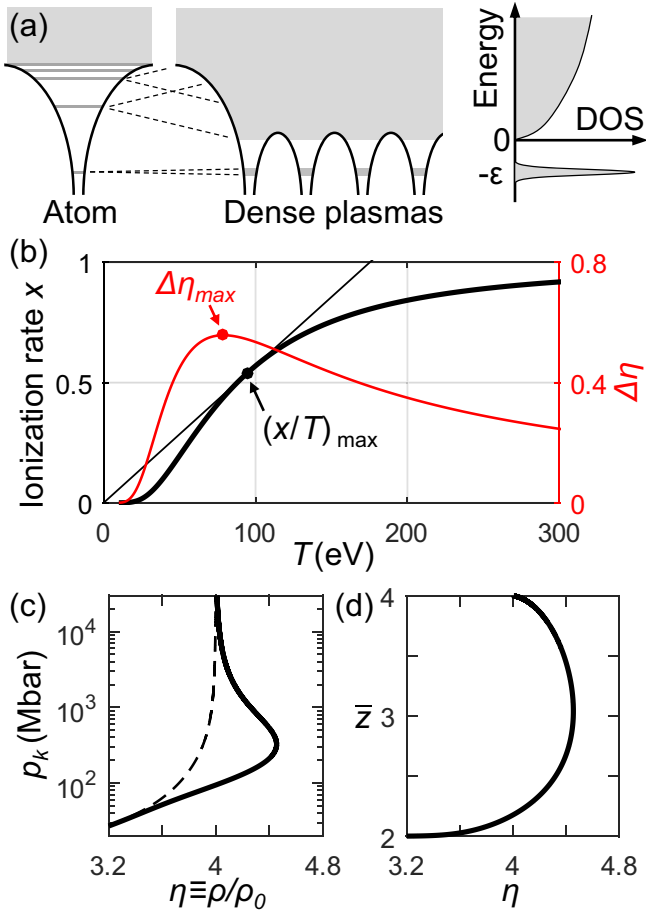


FIG. 1. A bound-state level introduces a peak in the Hugoniot upon ionization. (a) An illustration of the energy spectrum. Although the energy levels have shifted compared with the atomic levels, the overall structure remains: one (or more) bound-state level(s) resides beneath the continuum. (b) The ionization rate $x(T)$ increase monotonically along the Hugoniot, showing an “S-shaped” curve. Maximum compression ratio is related approximately to the point with maximum x/T , so $\Delta\eta$ has a peak. (c), (d) Pressure, compression ratio, and ionization rate along the principal Hugoniot of beryllium given by this model. The parameters used for panels (b)–(d) are $\varepsilon = 97.2$ eV, $z_0 = g = 2$, and $e_F^{(0)} = 14.7$ eV.

in most cases than pressure ionization or breaking chemical bonds, the following analysis focus primarily on thermal ionization.

Here, the bound state is treated as a discrete energy level with negligible broadening, and the free orbitals as ideal gas, as sketched in Fig. 1(a). Occupation of a bound state is given by

$$N_{e,b} \equiv Ng(1-x) = \frac{Ng}{1 + e^{(-\varepsilon - \mu)/T}}. \quad (1)$$

where N and $N_{e,b}$ are the numbers of atoms and bound electrons, $-\varepsilon$ is the bound-state energy, g is the degeneracy, and μ is the chemical potential which equals that of the free-electron gas. Since thermal ionization of the bound state is the process to be studied, the bound-state occupation number cannot be vanishingly small. So, describing the occupation with Fermi-Dirac distribution is necessary.

On the other hand, free electrons can be modeled classically—the temperature regime of interest here is on the order of the core-shell ionization energy, significantly larger than the corresponding Fermi energy.¹ The chemical potential of the free electrons, as a function of free electron density n_e and temperature T , is thus given by

$$n_e \equiv \frac{N_{e,f}}{V} \equiv \frac{N\bar{z}}{V} = 2 \left(\frac{m}{2\pi\hbar^2} \right)^{3/2} T^{3/2} e^{\mu(n_e, T)/T}. \quad (2)$$

Here, m is the mass of an electron, \hbar is the Planck constant, and the average ionic charge \bar{z} equals the number of initially free electrons per atom, z_0 , plus that from ionization: $\bar{z} = z_0 + gx$. We assume no ionization of core electrons at the initial state, so that the nucleus charge $Z = z_0 + g$.

To describe the Hugoniot adiabat, we have to study the energy difference between the pre- and postshock states. For the kinetic part, both ions and free electrons are effectively classical ideal gas for the postshock state, so their kinetic energy $E_k = (3/2)(1 + \bar{z})NT$. As for the preshock state, the free electron can be modeled as degenerate Fermi gas (especially for metals) and $E_k^{(0)} = (3/5)Nz_0e_F^{(0)}$ where $e_F^{(0)}$ is the initial-state Fermi energy.

The difference in potential energy takes a very simple form in the energy-band picture, which is the difference in bound-state electrons times the bound-state energy level $\Delta E_p = Ng\varepsilon x$. Other sophisticated terms, like the electron-electron interaction, exchange energy, etc., can largely be absorbed in the precise value of this ionization potential, as explained in Sec. IV and the Supplemental Material [21]. Therefore,

$$E - E^{(0)} = \frac{3}{2}(1 + \bar{z})NT + Ng\varepsilon x - E_k^{(0)}. \quad (3)$$

Postshock pressure can be well approximated it by its kinetic part $pV \approx (2/3)E_k$. And it is safe to ignore the initial-state pressure p_0 , since postshock pressure near the maximum compression ratio is usually several orders higher. Taken together, the Rankine-Hugoniot relation reads

$$E_k + Ng\varepsilon x - E_k^{(0)} = \frac{E_k}{3}(\eta - 1), \quad (4)$$

from which the compression ratio can be solved explicitly,

$$\eta = 4 + \frac{3g\varepsilon x}{E_k} - \frac{3E_k^{(0)}}{E_k}. \quad (5)$$

If without ionization of the bound electrons, the first and the third term on the right-hand side (r.h.s.) recapitulate the Hugoniot of ideal electron gas [22] that η increases monotonically and saturates at four, shown as the dashed curve in Fig. 1(c). With ionization, however, the additional ionization energy ($Ng\varepsilon x$) brings in the second positive term in Eq. (5). Denote this extra term as $\Delta\eta$,

$$\Delta\eta \equiv \frac{3g\varepsilon x}{E_k} = \frac{2g}{1 + \bar{z}} \frac{\varepsilon x}{T}. \quad (6)$$

¹For example, the principal Hugoniot of beryllium reaches its maximum compression ratio η_{\max} at ≈ 100 eV, while the Fermi energy e_F is ≈ 47 eV with three free electrons per atom at four times compression, thus $T/e_F \approx 2$. The energy difference due to degeneracy is less than 5%, which should not alter the main underlying physics here

We argue that Eqs. (5) and (6) have already contained the essential physics for the emergence of a peak in η along the Hugoniot. When the postshock temperature is low compared with ε , the ionization rate $x \sim e^{-\varepsilon/T}$ goes to zero, making $\Delta\eta \approx 0$ and the Hugoniot shows no deviation from ideal electron gas in the low-pressure region. At the other extreme, for very strong shocks with $T \gg \varepsilon$, ionization is nearly 100% ($x \approx 1$) and $\Delta\eta$ should decay with T as $\approx 1/T$. Since temperature increases monotonically along the Hugoniot curve,² the ionization rate x should always be an ‘‘S-shaped’’ function increasing monotonically from zero to saturation. The value of x/T thus show a peak in between, and so does $\Delta\eta$, see Fig. 1(b). Note that this argument for the presence of a peak is quite general and does not depend on the specific profile of the ‘‘S-shaped’’ ionization curve, nor on parameters like ε or g . There is also a universal feature implied by this argument that for $T \gg \varepsilon$, η scales as $(\eta - 4) \sim 1/T$.

With Eqs. (1) and (2), ionization rate x in the present model can be solved explicitly:

$$x = \left[1 + \frac{4\eta}{3\sqrt{\pi}} \frac{\bar{z}}{z_0} \left(\frac{e_F^{(0)}}{T} \right)^{3/2} e^{\varepsilon/T} \right]^{-1}. \quad (7)$$

Given the initial state, for each postshock temperature T , Eqs. (5)–(7) thereby determine a Hugoniot state in a self-consistent manner.

For example, the ionization energy of metallic beryllium $\chi = 111.5$ eV, which is measured from the bound state ($1s$ orbital, degeneracy $g = 2$) to the Fermi surface [24]. Thus, in our formalism we can take $-\varepsilon \approx e_F^{(0)} - \chi = -97.2$ eV and $z_0 = Z - g = 2$. With these parameters, Eqs. (5)–(7) give the self-consistent solution as solid lines in Figs. 1(b)–(d).

The ionization rate x along the Hugoniot indeed exhibits an S-shaped profile as in Fig. 1(b). Due to the prefactor $1/(1 + \bar{z})$ in Eq. (6), the maximum of x/T does not coincide precisely with the maximum of $\Delta\eta$; but the general picture is justified—the rise and fall of x/T leads to a peak of $\Delta\eta$. As expected, temperature at the peak is on the same order as ε , indicating that the peak is related to ionization. This point is also reflected by directly plotting x against η as in Fig. 1(d), that the η_{\max} -state corresponds to roughly 50% ionization.

At relatively lower temperatures, $T \sim e_F^{(0)}$, which is tens of eV here, the $E_k^{(0)}/E_k$ term in Eq. (5) is non-negligible that the peak smoothly ‘‘blends’’ into the sloped part of the Hugoniot [Fig. 1(c)]. This effect would significantly reduce the peak height if the ionization potential is not high enough compared with $E_k^{(0)}$ [like the M -shell peak of iron as in Fig. 3(d); see also the black curve in Fig. 2(a)]. Therefore in most cases, only the core electrons with high-enough ionization potentials contribute to the Hugoniot peak(s).

²This is true unless the Hugoniot crosses a phase boundary. An example of temperature decrease with η along the Hugoniot can be observed in the shock compression experiment of diamond carbon [23]. But the ionization peaks appear always at sufficiently high temperatures, away from all kinds of phase boundaries.

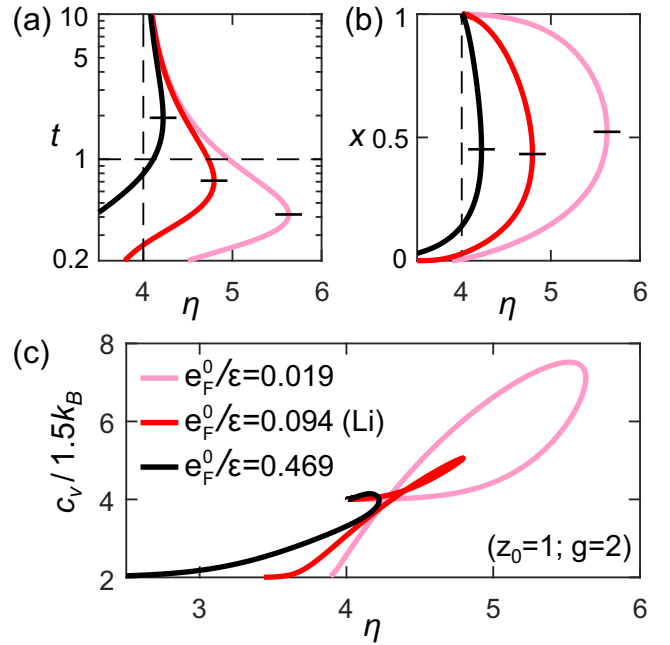


FIG. 2. Coincidences among the maximum compression ratio, max heat capacity, and 50% ionization are parameter dependent. $e_F^{(0)}/\varepsilon$ takes three different values here, 0.019 (pink), 0.094 which corresponds to lithium at normal density (red), and 0.469 (black); while z_0 and g are fixed to 1 and 2, respectively. (a) The temperature at η_{\max} can be higher or lower than the ionization potential depending on $e_F^{(0)}/\varepsilon$. (b) Ionization rate is close to 50% at η_{\max} but parameter dependence still exists. (c) For $e_F^{(0)}/\varepsilon$ different from that of normal-density lithium, the deviation between the max- c_v point and the max-compression point can also be significant.

III. SOME RULES OF THUMB AT η_{\max}

In the case of beryllium presented in Fig. 1, there seem to be some quantitative correlations near the maximum compression point. First, η_{\max} occurs at $T = 92.3$ eV, which is close to the ionization energy $|\varepsilon| = 97.2$ eV. Second, $\bar{z} = 3.05$ at η_{\max} , which is very close to the state where the K shell is half-ionized. Third, the maximum value of the heat capacity c_v along the Hugoniot appears at $\bar{z} = 2.83$, which is also close to the η_{\max} point. Qualitatively speaking, these coincidences are as expected—both the increments in compression ratio and in heat capacity beyond the ideal-gas limit originate from the underlying energy-absorbing process, which is ionization here. So they appear in roughly the same temperature range.

These ‘‘rules of thumb’’ are frequently discussed in the literature where principal Hugoniot are obtained using first-principle calculations [25–28]. In many cases they may even appear to be quantitatively precise, and people may wonder whether there exists any general underlying principle. However, with the model introduced here, we would like to clarify that there is no such simple universal argument—these rules actually depend on case-specific parameters such as initial density, ionization energy, and the numbers of free and bound electrons.

Our self-consistent model can be cast into a dimensionless form where the minimum number of model parameters are

kept. Define $t \equiv T/\varepsilon$:

$$x = \left[1 + \frac{4\eta}{3\sqrt{\pi}} \left(\frac{e_F^{(0)}}{\varepsilon} \right)^{3/2} \left(1 + \frac{gx}{z_0} \right) t^{-3/2} e^{1/t} \right]^{-1}, \quad (8a)$$

$$\eta = 4 + \frac{2gx/t}{1+z_0+gx} - \frac{6}{5} \left(\frac{e_F^{(0)}}{\varepsilon} \right) \frac{z_0/t}{1+z_0+gx}. \quad (8b)$$

The solution is completely determined by only three independent dimensionless parameters: the number of initial free electrons per atom, z_0 , the number of initially bound electrons (per atom), g , and the ratio between initial-state Fermi energy and the ionization energy $e_F^{(0)}/\varepsilon$, which reflects the initial density.

In Fig. 2 we study the influence of $e_F^{(0)}/\varepsilon$ on these three “rules” with z_0 fixed to 1 and g to 2. For metallic lithium, one has $\varepsilon = 50$ eV [24] and $e_F^{(0)} = 4.7$ eV, corresponding to the red curve in Fig. 2. The black curve, however, stands for a hypothetical material where the numbers of free and bound electrons are the same as lithium, but the ionization energy is artificially decreased (or equivalently, density is artificially increased), and vice versa for the pink curve. In the results, first, the temperature at maximum compression can be higher or lower than the ionization potential, depending on $e_F^{(0)}/\varepsilon$ [Fig. 2(a)]. Second, for lower (higher) $e_F^{(0)}/\varepsilon$, the maximum of c_v may come earlier (later) along the Hugoniot than the maximum of η [Fig. 2(c)]. And third, the ionization rate x at η_{\max} also changes, although not by a significant amount [Fig. 2(b)]. In short, all the three above-mentioned rules of thumb are compromised if initial density or ionization energy are altered; their seemingly widespread validity owns most likely to the fact that these dependencies are actually not quite sensitive, rather than some general underlying theory.

IV. MULTIPLE BOUND STATES

The present model can be extended straightforwardly to include multiple bound levels, as

$$pV = \frac{2}{3}E_k, \quad \Delta E = E_k - E_k^{(0)} + N \sum_i g_i \varepsilon_i x_i, \quad (9)$$

where $E_k = (3/2)(1 + \bar{z})NT$ as above. In parallel with Eqs. (3)–(5), since the nonkinetic part of energy difference is now a sum of contributions from different bound states, the $\Delta\eta$ term now becomes a summation over the bound levels, too. This leads to

$$\eta = 4 + \sum_i \Delta\eta_i - \frac{3E_k^{(0)}}{E_k}, \quad \Delta\eta_i = \frac{2g_i}{1 + \bar{z}} \frac{\varepsilon_i x_i}{T}. \quad (10)$$

Because the $\Delta\eta_i$ from different bound levels reach their peaks at different temperatures in general, the sum gives a Hugoniot with multiple peaks.

Although this general picture for multi-peaked Hugoniot is simple and clear, the exact values of the bound-state energies need more explanations. First, simply using the solid-state ionization energies (as done above for Li and Be) will lead to systematic underestimations. For example, the K -shell ionization energy for solid-state aluminum is measured when the L shell remains fully occupied, providing more screening than

in shock-compressed aluminum plasmas where the ionization of K electrons takes place with almost empty L shells. For single-shell elements like Li and Be, such differences vanish since there are no L shells. But it is no longer the case for multishell materials like aluminum or iron [21].

On the other hand, using ionization energies of isolated atoms would result in systematic overestimation. It is well known that the ionization energy in dense plasmas χ is lower than that of isolated atoms $\chi^{(\text{free})}$ due to electron-ion and electron-electron interactions. The difference is the so-called ionization potential depression (IPD). A simple estimation for IPD in dense plasmas could be $\chi^{(\text{free})} - \chi = (3/2)(\bar{z}/R)$ [29]. The equation is in atomic units and R is the radius of the ion sphere $(4\pi/3)R^3 \equiv V/N$. It can be shown using this estimation that simply ignoring IPD will also introduce considerable error (Fig. S1 in the Supplemental Material [21]).

Our goal is to model the difference in potential energy between the preshock state (ion charge $=z_0$) and the postshock state (ion charge $=z'$). To follow the energy band picture based on fixed energy levels, the shift of levels due to diminished screening and IPD are accounted for as follows: First, the energy difference is simply the sum of *successive ionization energies* $\Delta E_p = \chi_{z_0+1} + \dots + \chi_{z'}$. Then, in these successive ionization energies (χ_n), the effect of IPD should increase with ion charge n because the density of free electrons increases so there should be on average $n-1$ to n free electrons per atom in the entire plasma environment when the n th electron ionizes, and we take an intermediate value $n-1/2$.

Therefore, the energy levels are approximated as

$$\chi_n \approx \chi_n^{(\text{free})} - \frac{3}{2} \frac{4^{1/3}}{R_0} \left(n - \frac{1}{2} \right). \quad (11)$$

The successive ionization energies of isolated ions $\chi^{(\text{free})}$ are cited from the tables from National Institute of Standards and Technology (NIST) [32]. And IPD is estimated at $\eta \approx 4$, since most thermal ionizations relevant to the Hugoniot peaks take place at $\eta \approx 4$. Finally, the energy level for each of the bound electrons is defined as $-\varepsilon_n = -\chi_n$. In this way, the ionization potential in the energy-band picture reflects the total work against Coulomb potential for the n th electron to ionize, of which the sum gives the total increase in potential energy [21].

Although errors still exist for the above estimation of the ionization potential, Eq. (11) is good enough within the scope of the present work (as explained in the Supplemental Material [21]). For example, it gives $\varepsilon = 85.3$ and 121.7 eV for the two $1s$ electrons of Be, of which the mean value (103.5 eV) is very close to that used in Fig. 1 (97.2 eV), as expected.

For aluminum, the energy levels of the outermost three electrons go above the continuum after IPD correction, indicating that they are already free initially. The remaining 10 electrons ($1s^2, 2s^2, 2p^6$) are treated as bound electrons here. Their contributions add up to give two peaks. For iron, Eq. (11) sets the eight outermost electrons free (i.e., pressure ionized), thus a total of 18 bound electrons are considered for thermal ionization ($1s^2, 2s^2, 2p^6, 3s^2, 3p^6$). The principal Hugoniot for aluminum and iron calculated using Eqs. (7), (10), and (11) are shown in Figs. 3(a)–3(d). Values of the maximum compression ratio and the corresponding pressure (Al:

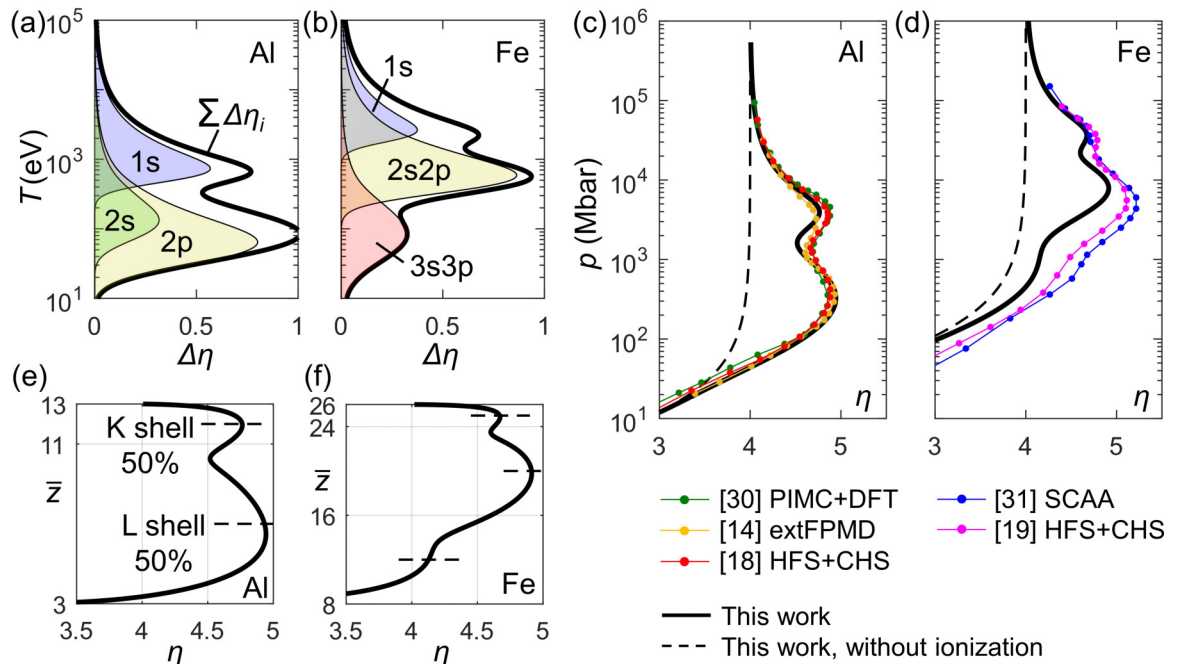


FIG. 3. Multiple bound-state levels lead to multiple peaks on the Hugoniot. (a) For Al, 10 core electrons from the $1s$, $2s$, and $2p$ subshells introduce $\Delta\eta$ peaks in different temperature ranges, yielding double-peaked Hugoniot when being summed. Contributions from each of the subshells is plotted separately. (b) Fe, the 18 core electrons from three different shells give three peaks in $\Delta\eta$. (c), (d) η - p Hugoniot for Al and Fe. The results (solid black curves) are obtained simply by adding the $\Delta\eta$ peaks shown in panels (a) and (b) to the “background” Hugoniot without ionization (dashed black lines). Several much more detailed first principles [14,30] and average atom model results [18,19,31] from the literature are also marked for comparison. (e), (f) Ionization rate along the principal Hugoniot, represented by averaged ion charge \bar{z} . The peaks in η appears to coincide roughly with 50% ionization of each of the core shells, as mentioned above. For Al, $\bar{z} = 7$ and 12 are marked with dashed bars. For Fe, the bars mark $\bar{z} = 12, 20$, and 25.

$\eta_{\max} = 4.94$, at 328 Mbar; Fe: $\eta_{\max} = 4.91$, at 7913 Mbar) and the main features of the Hugoniot profiles are basically consistent with those obtained by first-principles calculations [14,30] and detailed average atom models [18,19,31]. The remaining error should originate from our rough estimations of the energy levels rather than the overall picture [21].

Mean ion charges along the Hugoniot are given in Figs. 3(e) and 3(f), which reflect the ionization rate of each shell. Again, the maxima of compression ratio appear to coincide (but not precisely) with half filled shells.

Besides elements with multiple core shells as analyzed above, the picture that individual peaks are added linearly to give the overall increment in η applies to mixtures and compounds, too, where the bound-state levels may come from different types of atoms. In Fig. 4 we present result on aluminum oxide. Although the Hugoniot of pure aluminum displays two well-separated peaks, that of Al_2O_3 shows single-peak structure—simply because the K -shell peak of oxygen appears right between the two Al peaks. This feature is confirmed by recently published first-principles results [9], although the η_{\max} predicted here is slightly smaller.

Our model also offers a way to understand the Hugoniot of compounds (or mixtures) composed of mid- Z and very-low- Z elements, for instance LiF, H_2O , CH, etc. In those cases, the Hugoniot peak originates primarily from core electrons of the mid- Z atom. The very-low- Z atom species, which dissociates and fully ionizes much earlier than the main peak appears, provides only an “inert” background of the heat capacity.

Take CH plastic as an example. If without hydrogen, carbon with its fractional density $(12/13)\rho_0 = 0.97 \text{ g/cm}^3$ gives $\eta_{\max} = 1.76$ [Fig. 4(b), dotted green line]. However, hydrogen, which has become fully ionized at much lower temperature, gives two additional free particles per carbon atom. These additional particles modify the kinetic-energy term $E_k = (3/2)(1 + \bar{z} + 2)$, where \bar{z} is the average charge of carbon ions; hence $\Delta\eta$ [Fig. 4(b), dotted blue line]. These analyses are in good agreement with first-principles results [33].

V. ESTIMATING MAX COMPRESSION

The origin of the Hugoniot peaks have been explained above in a simple and general way. In this section, we would like to discuss the maximum achievable compression ratio along the principal Hugoniot. The maximum possible single-shock compression ratio is itself of general interest, and is also a natural test for the adequacy of our understandings for beyond-four-times compression. There exist some early attempts in providing such an upper bound through some general arguments [15,34], but their estimated bounds are rather loose (e.g., $\eta \leq 7$ according to Ref. [34]), and not based on an appropriate treatment of core-shell ionization.

To explore such global trends, in this section we ignore the initial-state kinetic energy $E_k^{(0)}$ completely, and further assume ionization to be *strictly sequential*, i.e., the $(z_0 + 1)$ st electron ionizes only after the ionization of all the previous

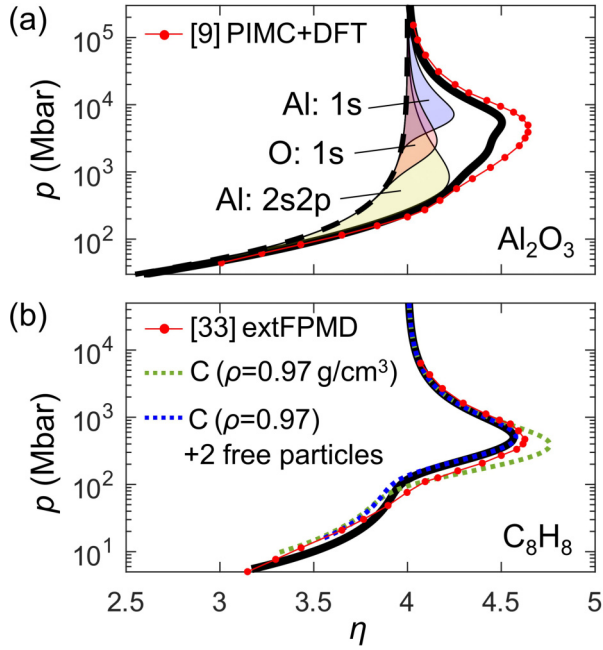


FIG. 4. Principal Hugoniot of compounds. (a) Aluminum oxide. Initial density $\rho_0 = 3.99 \text{ g/cm}^3$ following Ref. [9]. The Hugoniot obtained here (solid black curve) shows only one maximum in compression, because the oxygen K -shell peak lies just in between the two aluminum peaks. First principles calculation [9] shows the same feature. (b) CH plastic (polystyrene, C_8H_8) with initial density $\rho_0 = 1.05 \text{ g/cm}^3$. Our predicted Hugoniot (solid black curve) is consistent with first-principles results [33]. Dotted lines show that the carbon K -shell peak is modified due to the presence of hydrogen, as illustrated in the main text.

z_0 electrons have completed. These assumptions make the amount by which η exceeds four equal to the sum of $\Delta\eta_i$ from every *single* bound electron (per atom), and the latter can be studied independently. Setting $E_k^{(0)}$ to zero and replacing g by 1 in Eq. (8), one has

$$x = \left[1 + \frac{4\eta}{3\sqrt{\pi}} \alpha^{3/2} (z_0 + x)t^{-3/2} e^{1/t} \right]^{-1}, \quad (12a)$$

and

$$\eta = 4 + \frac{2}{1 + z_0 + x} \frac{x}{t}, \quad (12b)$$

which describes the $(z_0 + 1)$ st electron alone.

Only two effective parameters remained in Eq. (12), $\alpha \equiv e_F^{(0)}/\varepsilon z_0^{2/3}$ which represents the preshock density, and z_0 . Therefore, the entire parameter space can be explored and visualized exhaustively. The quantity of interest here is the maximum increment in η contributed by this single bound electron, $\delta\eta_m \equiv \max_t (\eta - 4)$, which is shown as the contour in Fig. 5.

At a first glance, very large compression ratio may seem to be allowed—by lowering both parameters, every single bound electron may contribute by as much as ≈ 2 or 3 to $\Delta\eta$. However, the parameter range for real solid-state materials is in fact strictly constrained. Consider the K shell as an example. For an average K electron, $z_0 = Z - 1$ is a good

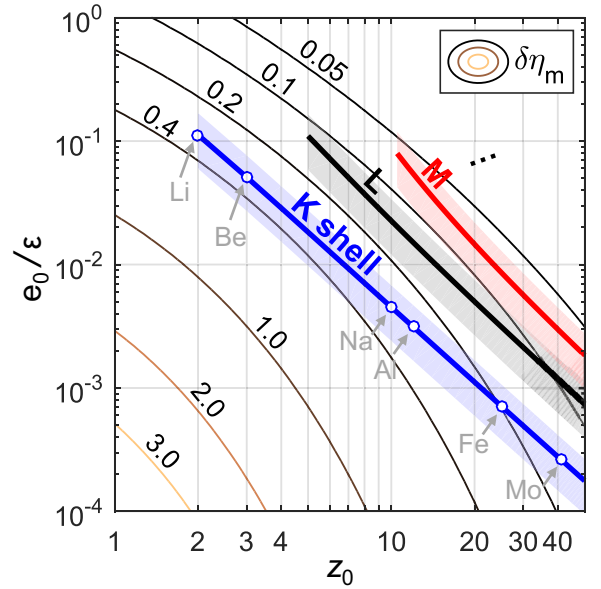


FIG. 5. The maximum increment in compression ratio due to single bound electron ($\delta\eta_m$, contour) depends on only two effective parameters according to Eq. (12). Estimations of the two parameters for realistic K -, L -, and M -shell electrons are shown as solid lines, with the atomic number Z increasing from the upper left to the lower right. Here, only the cases with $Z \geq 11$ are shown for the L shell, and $Z \geq 30$ for the M shell. Shaded regions marks the range $3.2 \text{ eV} < e_F^{(0)}/z_0^{2/3} < 9 \text{ eV}$.

estimation. As for the other parameter $\alpha \equiv e_F^{(0)}/\varepsilon z_0^{2/3}$, the characteristic energy $e_F^{(0)}/z_0^{2/3}$ reflects the initial atomic number density, it does not differ by orders of magnitude among solid-state materials. In most cases it lies between 3.2 eV (Na) to 9 eV (Be), hence choosing $e_F^{(0)}/z_0^{2/3} \approx 6 \text{ eV}$ would be reasonable. The K -shell ionization potential is approximately $\varepsilon \approx Z^2 \times 13.6 \text{ eV} - \Delta\chi^{\text{IPD}}$, and IPD here is roughly $\Delta\chi^{\text{IPD}} \approx (3/2)(4^{1/3}/R_0)(Z - 1)$ according to Eq. (11). Thus for a K -shell electron, the two parameters are effectively constrained on a one-dimensional curve as the nucleus charge Z varies:

$$\alpha \equiv \frac{e_F^{(0)}}{\varepsilon z_0^{2/3}} = \frac{0.27}{0.61Z^2 - Z + 1}, \quad z_0 = Z - 1. \quad (13)$$

This defines the blue line in Fig. 5 on which the points corresponding to different Z values are marked out for clarity. It is clear that the lower-left corner in Fig. 5 is actually unreachable for real solid materials.

A global trend is revealed as well. The K -shell peak height tends to decrease with increasing nucleus charge— $\delta\eta_m$ of a K -shell electron decreases from ≈ 0.4 for Li and Be to ≈ 0.15 for Mo. This is consistent with the literature that claims that the K -shell peak becomes hardly visible for high- Z materials [8,35] as well as with our previous results in Figs. 3(a) and 3(b) that the K -shell peak of iron is visibly smaller than that of aluminum. Mathematically, this trend can be traced back to the $(1 + z_0 + x)^{-1}$ factor in Eq. (12b)—the larger is Z , the smaller this prefactor. Intuitively, for $z_0 \gg 1$ the kinetic energy of the existing free electrons become overwhelmingly

high compared with the energy cost to ionize another K -shell electron.

This trend holds also for L - and M -shell electrons which are shown as the black and red curves in Fig. 5. In general, a single L - or M -shell electron does not contribute as much to compression ratio as a K electron because its ionization energy is much lower. However, these outer shells contain more electrons in general. This makes their *overall* contributions to compression ratio, which is roughly the number of electrons times $\delta\eta_m$, become comparable or even more significant than the K shell. This is especially true for high- Z materials.

For example, for iron ($Z = 26$) an average K -, L -, or M -shell electron has $\delta\eta_m \approx 0.2, 0.12$, or 0.04 , as estimated here. The number of bound electrons in them are 2, 8, and 8, respectively. Therefore, the shell-summed $\Delta\eta$ ($\approx N\delta\eta_m$) should be 0.4, 1.0, and 0.3 for the K -, L -, and M -shell, respectively. So, η_{\max} is reached by the L -shell peak, as shown in Fig. 3(b). For lead ($Z = 82$), $\delta\eta_m$ again decreases with the shell number, $\approx 0.11, 0.08, 0.07, 0.05$ for the K, L, M , and N shells. However, since the number of electrons in these shells increases rapidly (2, 8, 18, and 32), the N -shell peak would be the highest.

Therefore, there are two competing global tendencies as Z increases—contribution by a *single* electron from a given shell tends to decrease with Z and with the shell quantum number n ; while the *total number* of bound electrons increases rapidly with n , making η_{\max} tend to be reached by higher- n shells for higher- Z materials. These two competing trends have several implications. First, the value of η_{\max} increases very slowly with Z : from ≈ 5 (Al) to ≈ 6 (Pb) for solids. Second, although ionization energy of a given shell increases rapidly with Z , that of *the* shell responsible for maximum compression correlates only weakly with Z , as has been discussed with a summary of the numerical results [9].

Besides that η_{\max} increases slowly with Z , the contour in Fig. 5 also implies that higher compression ratio can be reached by starting from lower initial density. Decrease in initial density leads to a decrease in $e_F^{(0)}$ (while z_0 and ε remain largely unchanged), which corresponds to moving vertically downward in Fig. 5, i.e., up the contour of $\delta\eta_m$. Thus, lower (higher) initial density leads to higher (lower) maximum compression ratio in general. This tendency has been repeatedly demonstrated by experiments and first-principles calculations [13,26,27]. And single-shock compression ratios of around 7–8 are reported for low-density foams experimentally [36,37].

It can be read from Fig. 5 that $\delta\eta_m$ scales as $-\ln\alpha$ (hence $-\ln\rho_0$) since the contour is roughly equally spaced while α is in log scale. Therefore, although achieving arbitrarily large compression ratio with arbitrarily low initial density may seem to be possible theoretically, this logarithmic divergence is extremely slow. Even for foam with $\approx 1/10$ solid-state density, a single shock can compress it for no more than ≈ 7 times, as predicted here³. (Fig. 6).

³This analysis applies only to shocks strong enough to vaporize or ionize the foam. Because in Eq. (12) we are assuming the increment in thermal energy is directly related to the increment in pressure. Especially, this analysis may not apply to mechanical crushing of foams with very high porosity

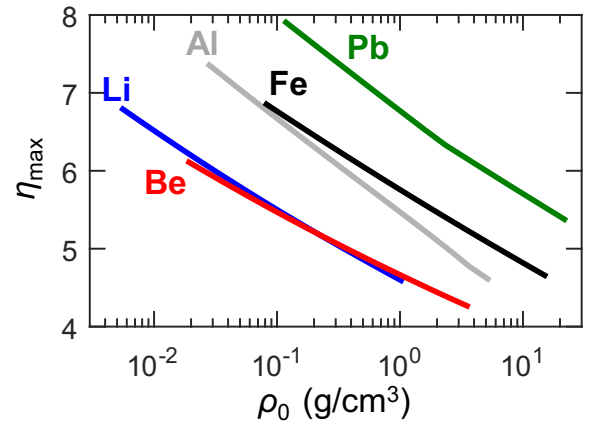


FIG. 6. Maximum single-shock compression ratio decreases with the preshock density ρ_0 . Results for Li, Be, Al, Fe, and Pb are obtained using the same set of equations as in Fig. 3. ρ_0 range from 0.01 to 2 times the solid-state density.

VI. DISCUSSION

A. Corrections on ideal-gas pressure

Many features concerning the peaks on the Hugoniot adiabat are successfully captured by the simple model presented above, and the underlying mechanism is clearly revealed and shown to be general. This success should own mainly to the energy terms we have used. The energy difference can in principle be well modeled by the energy-band picture if provided with a satisfactory estimation of IPD.

However, the pressure term we have used above includes only the kinetic term. This approximation in pressure is necessary for us to introduce the decomposition of $\Delta\eta$ as Eq. (10), thereby making the overall picture simple. In this section, we show that the neglected nonkinetic pressure term indeed has little effect.

The situation here resembles very much the well-known paradox in metals, where the Coulomb interaction seems to be so strong but the conduction electrons can still be treated as near-free. The key point is that core repulsion effect due to wave function orthogonalization has largely compensated the electron-ion attraction [38,39]. In this spirit, the Coulomb energy for an average ion is (following Ref. [38])

$$E_C = -\frac{3}{4\pi} \left(\frac{9\pi}{4} \right)^{1/3} \frac{\bar{z}^{4/3}}{R} - \frac{9}{10} \frac{\bar{z}^2}{R} + \frac{3}{2} \frac{\bar{z}^2 R_c^2}{R^3} \quad (\text{a.u.}) \quad (14)$$

The three terms above are the exchange energy, classical Coulomb attraction, and core repulsion with R_c being the ion core radius. The Coulomb interaction contributes to the total pressure by $p_c = -\partial E_C / \partial V$, therefore,

$$p_c V = -\frac{3\bar{z}^2}{2R} \left[\frac{1}{4\pi} \left(\frac{9\pi}{4} \right)^{1/3} \bar{z}^{-2/3} + \frac{1}{5} - \left(\frac{R_c}{R} \right)^2 \right], \quad (15)$$

where V is the volume of an average ion.

As an example, for aluminum near the maximum compression state, we have $\eta = 4.9$ and $\bar{z} = 7$ according to Fig. 3(e), thus $R = 1.75$ bohr. The radius of an Al^{7+} ion is roughly 0.8 bohr, defined as enclosing 90% of the L -shell electron density. Therefore, the pressure modification due to exchange

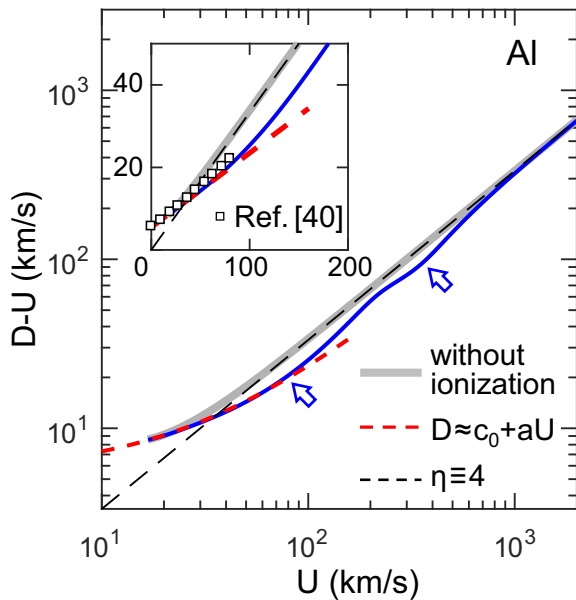


FIG. 7. Hugoniot peaks of aluminum in terms of the shock and particle velocities D and U . The solid blue curve given by Eq. (18) represents the same calculated Hugoniot states as the black curve in Fig. 3(c). The K - and L -shell peaks are marked with arrowheads. The dashed red line is a linear fitting to the Hugoniot adiabat obtained in this work, with $c_0 = 5.5$ km/s and $a = 1.18$. The inset shows the same plot on a linear scale. Open squares mark a high-precision quadratic fitting to experimental data [40].

energy, classic Coulomb attraction, and core repulsion are -14.9 , -107.3 , and $+110.8$ Mbar, respectively, which sums up to give only -11.4 Mbar. Note that kinetic pressure at this condition is $+348$ Mbar. The compression ratio η would be perturbed by $(1 - \eta)p_C/p_k \approx +0.13$ due to the modification in pressure. η_{\max} thus changes from ≈ 4.9 to ≈ 5.0 , which is indeed a small modification in the scope of the present paper.

B. Hugoniot peaks in the D - U representation

In many cases [36,40] the shock Hugoniot is studied in terms of the shock velocity D and corresponding particle velocity behind the shock front U . So it worth studying how the peak structures in η are reflected in the D - U plot. For stationary zero-pressure samples compressed by a single shock, the increase of internal energy always equals to the increase of bulk kinetic energy.

$$\Delta E = E_k + N \sum g_i \varepsilon_i x_i - E_k^{(0)} = Nm \frac{U^2}{2}, \quad (16)$$

where m is the atomic mass. On the other side, using the relations $p = \rho_0 D U$ and $\eta = D/(D - U)$, we have

$$pV = NmU(D - U). \quad (17)$$

Substituting pV with $(2/3)E_k$ and eliminating E_k , Eqs. (16) and (17) finally yield

$$D = \frac{4}{3}U + \frac{2e_k^{(0)}}{3U} - \frac{2 \sum g_i \varepsilon_i x_i}{3U}. \quad (18)$$

Here, $e_k^{(0)} \equiv E_k^{(0)}/Nm$, $\varepsilon_i \equiv \varepsilon_i/m$. This result has very similar form as Eq. (10), that the three r.h.s terms correspond to $\eta = 4$, initial energy, and the sum of ionization peaks, respectively. Note that the peaks in shock velocity D are negative, indicating greater compressibility.

Note that Eq. (18) is not applicable to very weak shocks because it diverges when U approaches zero. This is because the approximation $p \approx p_k$ brings in huge relative error as $U \rightarrow 0$. Despite this, the well-known linear relationship between D and U for solid materials is reproduced here for a wide range of U (Fig. 7, dashed red line). This linear relationship remains valid even up to $\eta \approx 4.5$, in agreement with Ref. [40] where linear D - U relation plus a very small quadratic term provides high-precision fitting to experimental data before the Hugoniot turns back.

VII. CONCLUSION

Along the Hugoniot adiabat, some internal degrees of freedom are excited as temperature rises, making the compression ratio go beyond four. This is a general feature for the shock Hugoniot of all materials. We provide an explanation for it which takes into account only the minimum necessary physics but provides a fairly satisfactory accuracy. We show that a positive additional energy term besides the kinetic energy is directly related to a peak in compression ratio η on the Hugoniot. In most cases, this term is the ionization energy of bound electrons. The increment in η due to different bound electrons are shown to add linearly as $\eta \approx 4 + \sum \Delta \eta_i$, giving the Hugoniot with multiple peaks. This general picture explains in a natural way many global trends in which η_{\max} varies with nucleus charge Z . Also, the ‘‘rules of thumb’’ among η_{\max} , $c_{v \max}$, and 50% ionization states are reproduced and discussed. The present results have clearly resolved the origin of the peak structures of the Hugoniot and clarified some of the important effects and relevant energy scales in this regime. This may help us to better understand results from theoretical calculations and experiments.

ACKNOWLEDGMENTS

We thank Yutong Yang, Chongjie Mo, and Xiaohan Zhang for helpful discussions.

- [1] R. Betti and O. Hurricane, Inertial-confinement fusion with lasers, *Nat. Phys.* **12**, 435 (2016).
 [2] E. Campbell, V. Goncharov, T. Sangster, S. Regan, P. Radha, R. Betti, J. Myatt, D. Froula, M. Rosenberg, I. Igumenshchev *et al.*, Laser-direct-drive program: Promise,

challenge, and path forward, *Matter Radiat. Extremes* **2**, 37 (2017).

- [3] R. Treumann, Fundamentals of collisionless shocks for astrophysical application, 1. non-relativistic shocks, *Astron. Astrophys. Rev.* **17**, 409 (2009).

- [4] P. Wang, C. Zhang, S. Jiang, X. Duan, H. Zhang, L. Li, W. Yang, Y. Liu, Y. Li, L. Sun, H. Liu, and W. Zhebin, Density-dependent shock Hugoniot of polycrystalline diamond at pressures relevant to ICF, *Matter Radiat. Extrem.* **6**, 035902 (2021).
- [5] Y. B. Zeldovich and Y. P. Raiser, *Physics of Shock Waves and High Temperature Hydrodynamic Phenomena* (Academic Press, New York, 1966), Vol. 1.
- [6] H. Liu, W. Kang, Q. Zhang, Y. Zhang, H. Duan, and X. T. He, Molecular dynamics simulations of microscopic structure of ultra strong shock waves in dense helium, *Front. Phys.* **11**, 115206 (2016).
- [7] L. B. Da Silva, P. Celliers, G. W. Collins, K. S. Budil, N. C. Holmes, T. W. Barbee Jr., B. A. Hammel, J. D. Kilkenny, R. J. Wallace, M. Ross, R. Cauble, A. Ng, and G. Chiu, Absolute Equation of State Measurements on Shocked Liquid Deuterium up to 200 GPa (2 Mbar), *Phys. Rev. Lett.* **78**, 483 (1997).
- [8] B. F. Rozsnyai, J. R. Albritton, D. A. Young, V. N. Sonnad, and D. A. Liberman, Theory and experiment for ultrahigh pressure shock Hugoniots, *Phys. Lett. A* **291**, 226 (2001).
- [9] B. Militzer, F. González-Cataldo, S. Zhang, K. P. Driver, and F. Soubiran, First-principles equation of state database for warm dense matter computation, *Phys. Rev. E* **103**, 013203 (2021).
- [10] M. Ross, Linear-mixing model for shock-compressed liquid deuterium, *Phys. Rev. B* **58**, 669 (1998).
- [11] M. D. Knudson, D. L. Hanson, J. E. Bailey, C. A. Hall, and J. R. Asay, Use of a Wave Reverberation Technique to Infer the Density Compression of Shocked Liquid Deuterium to 75 GPa, *Phys. Rev. Lett.* **90**, 035505 (2003).
- [12] H. Liu, Y. Zhang, W. Kang, P. Zhang, H. Duan, and X. T. He, Molecular dynamics simulation of strong shock waves propagating in dense deuterium, taking into consideration effects of excited electrons, *Phys. Rev. E* **95**, 023201 (2017).
- [13] B. Militzer, First Principles Calculations of Shock Compressed Fluid Helium, *Phys. Rev. Lett.* **97**, 175501 (2006).
- [14] S. Zhang, H. W. Wang, W. Kang, P. Zhang, and X. T. He, Extended application of Kohn-Sham first-principles molecular dynamics method with plane wave approximation at high energy—from cold materials to hot dense plasmas, *Phys. Plasmas* **23**, 042707 (2016).
- [15] J. C. Pain, Equation-of-state model for shock compression of hot dense matter, *Phys. Lett. A* **362**, 120 (2007).
- [16] G. Faussurier, C. Blancard, and P. Renaudin, Equation of state of dense plasmas using a screened-hydrogenic model with ℓ -splitting, *High Energy Density Phys.* **4**, 114 (2008).
- [17] M. R. Zaghoul, Critical parameters, thermodynamic functions, and shock Hugoniot of aluminum fluid at high energy density, *High Energy Density Phys.* **26**, 8 (2018).
- [18] M. A. Kadatskiy and K. V. Khishchenko, Comparison of Hugoniots calculated for aluminum in the framework of three quantum-statistical models, *J. Phys.: Conf. Ser.* **653**, 012079 (2015).
- [19] M. A. Kadatskiy and K. V. Khishchenko, Shock compressibility of iron calculated in the framework of quantum-statistical models with different ionic parts, *J. Phys.: Conf. Ser.* **774**, 012005 (2016).
- [20] R. P. Drake, *High Energy Density Physics—Fundamentals, Inertial Fusion, and Experimental Astrophysics* (Springer Science & Business Media, Berlin, 2006).
- [21] See Supplemental Material at <http://link.aps.org/supplemental/10.1103/PhysRevB.107.035102> for a discussion on our treatments of the bound state energy levels and the approximations involved. See also Refs. [41,42] herein.
- [22] W. J. Nellis, Shock compression of a free-electron gas, *J. Appl. Phys.* **94**, 272 (2003).
- [23] J. Eggert, D. Hicks, P. Celliers, D. Bradley, R. McWilliams, R. Jeanloz, J. Miller, T. Boehly, and G. Collins, Melting temperature of diamond at ultrahigh pressure, *Nat. Phys.* **6**, 40 (2010).
- [24] A. Thompson, D. Attwood, E. Gullikson, M. Howells, K. Kim, J. Kirz, J. Kortright, I. Lindau, Y. Liu, P. Pianetta, A. Robinson, J. Scofield, J. Underwood, G. Williams, and H. Winick, *X-Ray Data Booklet*, 3rd ed. (Lawrence Berkeley National Laboratory, Berkeley, California, 2009).
- [25] K. P. Driver, F. Soubiran, S. Zhang, and B. Militzer, First-principles equation of state and electronic properties of warm dense oxygen, *J. Chem. Phys.* **143**, 164507 (2015).
- [26] K. P. Driver and B. Militzer, First-principles equation of state calculations of warm dense nitrogen, *Phys. Rev. B* **93**, 064101 (2016).
- [27] S. Zhang, K. P. Driver, F. Soubiran, and B. Militzer, Equation of state and shock compression of warm dense sodium—a first-principles study, *J. Chem. Phys.* **146**, 074505 (2017).
- [28] C. Gao, S. Zhang, W. Kang, C. Wang, P. Zhang, and X. T. He, Validity boundary of orbital-free molecular dynamics method corresponding to thermal ionization of shell structure, *Phys. Rev. B* **94**, 205115 (2016).
- [29] J. C. Stewart and K. D. Pyatt Jr, Lowering of ionization potentials in plasmas, *Astrophys. J.* **144**, 1203 (1966).
- [30] K. P. Driver, F. Soubiran, and B. Militzer, Path integral Monte Carlo simulations of warm dense aluminum, *Phys. Rev. E* **97**, 063207 (2018).
- [31] B. F. Rozsnyai, Shock Hugoniots based on the self-consistent average atom (SCAA) model, theory and experiments (second revision), *High Energy Density Phys.* **8**, 88 (2012).
- [32] A. Kramida, Ralchenko, J. Yu., Reader, and N. A. Team, NIST atomic spectra database (version 5.9), <https://www.nist.gov/pml/atomic-spectra-database>, accessed Jan 12 (2022).
- [33] X. Liu, X. Zhang, C. Gao, S. Zhang, C. Wang, D. Li, P. Zhang, W. Kang, W. Zhang, and X. T. He, Equations of state of poly- α -methylstyrene and polystyrene: First-principles calculations versus precision measurements, *Phys. Rev. B* **103**, 174111 (2021).
- [34] J. D. Johnson, Bound and estimate for the maximum compression of single shocks, *Phys. Rev. E* **59**, 3727 (1999).
- [35] M. A. Kadatskiy, Quantum-statistical calculations of the thermodynamic properties of molybdenum at high energy densities, *High Energy Density Phys.* **33**, 100700 (2019).
- [36] *LASL Shock Hugoniot Data* (University of California Press, Berkeley, Los Angeles, 1980).
- [37] Y. Aglitskiy, A. L. Velikovich, M. Karasik, A. J. Schmitt, V. Serlin, J. L. Weaver, J. Oh, S. P. Obenschain, and K. R. Cochrane, Absolute Hugoniot measurements for CH foams in the 2-9 Mbar range, *Phys. Plasmas* **25**, 032705 (2018).
- [38] R. M. Martin, *Electronic Structure* (Cambridge University Press, Cambridge, 2004).

- [39] N. W. Ashcroft and N. D. Mermin, *Solid State Physics* (World Publishing Corp., Beijing, 2004).
- [40] L. V. Al'tshuler, N. N. Kalitkin, L. V. Kuz'mina, and B. S. Chekin, Shock adiabats for ultrahigh pressures, *Sov. J. Exp. Theor. Phys.* **45**, 167 (1977).
- [41] R. M. More, Pressure ionization, resonances, and the continuity of bound and free states, *Adv. At. Mol. Phys.* **21**, 305 (1985).
- [42] M. Natapoff, Calculation of the atomic radius from shielding considerations, *J. Phys. Chem. Solids* **37**, 59 (1976).